

# Impact of Late Quaternary climatic fluctuations on coastal systems: Evidence from high-resolution geophysical, sedimentological and geochronological data from the Java Island

Novico Franto <sup>1,2</sup>, Menier David <sup>3,\*</sup>, Mathew Manoj <sup>4</sup>, Ramkumar Mu <sup>5</sup>, Santosh M. <sup>6,7</sup>, Endyana Cipta <sup>1</sup>, Dewi Kresna Tri <sup>8</sup>, Kurniawan Indra <sup>9</sup>, Lambert Clement <sup>3</sup>, Goubert Evelyne <sup>3</sup>, Hendarmawan <sup>1</sup>

<sup>1</sup> Department of Engineering Geology, Padjadjaran University, 45363, Jatinangor, Indonesia

<sup>2</sup> Marine Geological Research and Development Center, Ministry of Energy and Mineral Resources, 40174, Bandung, Indonesia

<sup>3</sup> Laboratoire Géoscience Océan, UMR CNRS 6538, Université Bretagne Sud, 56017, Vannes, France

<sup>4</sup> Laboratoire Géoscience Océan, UMR CNRS/UBO/UBS 6538, IUEM, Université de Brest, 29280, Plouzané, France

<sup>5</sup> Department of Geology, Periyar University, 636011, Salem, India

<sup>6</sup> Department of Earth Sciences, University of Adelaide, Adelaide, SA, 5005, Australia

<sup>7</sup> Beijing School of Earth Sciences and Resources, China University of Geosciences, 100083, Beijing, China

<sup>8</sup> Center of Geological Survey, Ministry of Energy and Mineral Resources, 40122, Bandung, Indonesia

<sup>9</sup> Directorate of Water Resources, Ministry of Public Works and Housing, 12110, Jakarta, Indonesia

\* Corresponding author : David Menier, email address : [david.menier@univ-ubs.fr](mailto:david.menier@univ-ubs.fr)

## Abstract :

The major climatic oscillations during the Quaternary Period significantly influenced the evolution and distribution of ancient and modern coastal systems. Here we investigate the morphology and sedimentary infilling of submerged Late Quaternary incised valleys along the northern coast of Java Island (Indonesia) using high-resolution geophysical, sedimentological and geochronological data. Our results indicate that the spatial development and morphology of the incised valleys are predominantly controlled by Quaternary glacial-interglacial eustatic fluctuations, within a marked subsiding setting. The valleys were incised during prominent Quaternary lowstands and most of the valley fill was emplaced during the last postglacial sea level rise. The valley fill forms a transgressive succession, consisting mainly of fluvial deposits at the base (possibly amalgamated from older sequences) overlain by shallow marine sediments and capped by hemipelagic deposits. The valley-fill architecture is strongly dependent on the valley morphology (depth of incision, width of the valleys, and extent of the intertidal zone). The shallow marine deposits contained within the narrow and linear valleys are mostly aggrading muds. The vertical incision and valley formation was chiefly controlled by the extent of glacial sea-level fluctuations. The studied sections represent the continental-offshore extension of a paleodeltaic system. The implication of our work is that even in predominantly enclosed shallow marine systems that are located distal to the shelf

---

break, the response of the sedimentary system and ensuing stratigraphic configuration can be effectively impacted by the rapid and abrupt Quaternary global climatic transition and eustatic sea-level fluctuations.

### Highlights

► Java Quaternary incised valley-fill consists of fluvial deposits at the base overlain by estuarine sediments and capped by hemipelagic deposits. ► The studied sections represent continental-offshore extension of the paleodeltaic system. ► Late Quaternary climatic and eustatic changes impacted sedimentary framework of enclosed shallow marine systems located distal to shelf break.

**Keywords** : Last glacial maximum, Java sea, Incised valleys, Depositional controls, Stratal morphology

## 1. Introduction

48 The Quaternary Period is characterized by rapid, large-scale and abrupt climatic oscillations  
49 that strongly influenced the evolution and distribution of ancient coastal systems around the  
50 world and continue to exert control until present-day (Adams et al., 1999; Elias, 2013;  
51 Gornitz, 2021). The associated eustatic fluctuations predominantly generated arrays of incised  
52 valleys during relative sea level lowstands which were inundated and filled during subsequent  
53 relative sea level rise, inundated and infilled the incised valleys. Over the last 40 years, owing  
54 to its scientific and economic significance, extensive research has been focused on the  
55 stratigraphy and infilling of such incised valleys or paleochannels (Puchala et al., 2011; Wang  
56 et al., 2020). Research conducted elsewhere has provided important geomorphologic as well  
57 as stratigraphic information from regions such as the North and South American shelf (e.g.,  
58 Dalrymple et al., 1994; Nordfjord et al., 2006; Moreira et al., 2019), northwest European shelf  
59 (e.g., Allen and Posamentier, 1993 and 1994; Tesson et al., 2000; Chaumillon et al., 2010;  
60 Menier et al., 2010; Martinez-Carreno and Garcia-Gil, 2017), northeastern Australian shelf  
61 (e.g., Fielding et al., 2005), southwestern Huanghai shelf (e.g., Kong et al., 2011), South  
62 African shelf (e.g., Green, 2009), eastern Indian coast (e.g., Dubey et al., 2019), Sunda shelf  
63 in Southeast Asia (e.g., Hanebuth et al., 2009; Puchala et al., 2011; Horozal et al., 2021),  
64 among others.

65 In Southeast Asia, the Sunda Shelf or Sundaland is an extension of the continental shelf and  
66 includes the island of Java, the Malay peninsula, Sumatra, Borneo, Madura, Bali and their  
67 surrounding smaller islands. It covers an area of approximately 1.85 million km<sup>2</sup>. Its seas are  
68 relatively shallow and was exposed several times during the Pleistocene (e.g., Emery et al.,  
69 1972; Hanebuth et al., 2009) when Sumatra, Java, Borneo and the Malay peninsula were  
70 connected and formed a single large landmass (Heaney et al., 1991; Voris, 2000; Bird et al.,  
71 2005) (Fig. 1A). During the Last Glacial Maximum (LGM), ~26.5–19 ka BP, much of the  
72 remaining Sundaland area was covered by savanna, grassland, lowland evergreen forests,

73 marshy grounds and crossed axially by the deeply incised ‘rivers’ feeding the late falling-  
74 stage deltas that debouched close to the present-day shelf break of the Sundaland (Hanebuth  
75 et al., 2009; Hanebuth et al., 2011; Puchala et al., 2011; Sathiamurthy and Rahman, 2017;  
76 Irwanto, 2019). The Java Sea that today corresponds to a large and shallow sea of the Sunda  
77 Shelf, which lies between the islands of Borneo to the north, Java to the south, Sumatra to the  
78 west and Sulawesi to the east, was entirely exposed during the LGM (Clark et al., 2009). The  
79 Java Sea was occupied by river valleys and channels that coursed to the shelf break located  
80 toward the eastern part of Java. Currently, the northwestern region of the Java Sea hosts a  
81 poorly-documented offshore sedimentary prism dominated by argillaceous deposits within a  
82 rapidly subsiding geodynamic setting (Abidin et al., 2008, 2013 and 2015, Chaussard et al.,  
83 2013; Husson et al., 2019). While it is recognized that this region has undergone various  
84 phases of tectonic and eustatic fluctuations until recent-times (e.g., Zahirovic et al., 2016), a  
85 detailed analysis of the sedimentary architecture and stratigraphic archive, which can  
86 potentially encapsulate evidences of important environmental changes in response to  
87 endogenic and exogenic forcing, remain less understood.

88 Here, we present a detailed description of the shallow sub-bottom stratigraphy of the offshore  
89 section of northwest Java (Fig. 1B) using results obtained from shallow seismic surveys and  
90 cores collected in 2015. These results, aided with radiocarbon ages provide insights into the  
91 Pleistocene to Holocene transition events and the major climatic and eustatic controls on the  
92 sedimentary organization within a subsiding shelf setting.

## 93 **2. Geological characteristics of Java and Java Sea**

### 94 **2.1. Structural setting**

95 Sundaland consists of a stable core of Paleozoic continental crust that was augmented in size  
96 by tectonism and volcanism associated with subduction along the southern margin of the

97 continent, with episodes of uplift and subsidence affecting the entire Sunda Shelf (Bird et al.,  
98 2005; Metcalfe, 2011). Java represents a volcanic arc built on the southernmost margin of the  
99 continental Sunda Plate, due to the subduction of the oceanic Australia-Indian plate (Fig. 2A;  
100 Hamilton, 1979). It is a structurally complex island attributable to a long history of accretion  
101 of Gondwana-derived crustal blocks that led to a configuration of alternating highs and  
102 transverse depressions (Haberland et al. 2014). The northern part of the Northwest Java Basin,  
103 including the coastal area, is dominated by extensional faulting with minimal compressional  
104 structures (Darman and Sidi, 2000; Sathiamurthy et al., 2006). It was formed by continuous  
105 subsidence and southward tilting of the Sunda Plate since the Paleogene (Hamilton, 1979).  
106 The subsidence is documented to have resulted in the development of the Pulau Seribu  
107 carbonate platforms (Fig. 1B) and the NE-SW trending asymmetrical northwest Java basinal  
108 area (Suyanto et al., 1977). Subsequent development of several sub-basins and basement  
109 highs within the basin (Patmosukismo et al., 1974) was associated with N-S trending block  
110 faulting (Adriansyah et al., 2002).

## 111 **2.2. Geomorphology and seafloor sedimentary cover**

112 Morphologically, the Java Sea is roughly rectangular in shape, located between Sumatra to the  
113 west and Bali to the east. In the west, it is open to the Indian Ocean through the Sunda Strait  
114 and the Karimata Strait, respectively. In the east, it has an open connection to the Flores Sea  
115 and the Sulawesi Sea through the Makassar Strait (Durand & Petit, 1995; Genia et al., 2007).  
116 The Java Sea including Jakarta Bay is a large (~310,000 km<sup>2</sup>), shallow sea (40–100 m water  
117 depth) and the slope is toward the east at the edge of the Sunda Shelf. Seafloor surface  
118 sediment of Indonesian waters including the Java Sea generally consists of cohesive fine-  
119 grained sediments (Fig. 2).

120 Java presents an elongated morphology with a surface area of ~130,000 km<sup>2</sup> (~1000 km in  
121 length and ~210 km wide). The coastline is structurally controlled and shows an irregular

122 morphology. Northern Java including the Jakarta Bay is in a transition area between the  
123 volcanic arc and the extensional back-arc zone. This area is characterized by the flat alluvial  
124 plain of the coastal zone. The southern parts of Java are occupied by volcanic mountains  
125 where Mount Semeru is the highest (~36576 m). Java is drained by multiple rivers, with large  
126 drainage basins in the north and small drainage basins in the south (Figure 3). The drainage  
127 pattern is predominantly controlled by the volcanic arc and recent uplift (Marliyani, 2016).

### 128 **2.3. Sea level changes**

129 On a global scale, the development of Quaternary stratigraphy of continental shelves was  
130 predominantly controlled by glacio-eustatic fluctuations (Suter et al., 2012). Hence, an  
131 understanding of relative sea-level change may help to explain critical interactions in earth  
132 environmental systems throughout the Quaternary (Shennan, 2018).

133 The Sundaland core is considered to be tectonically quiescent, as evidenced by the lack of  
134 noticeable seismic activity of the fault systems. However, a recent biographical study on  
135 organism divergence time (Husson et al., 2019) shows that Sundaland was subaerially  
136 exposed before 400 ka and subsequently experienced subsidence at a rate of 0.2–0.3 mm yr<sup>-1</sup>  
137 (Sarr et al., 2019). The insights gained from Sarr et al. (2019), resulted in an updated  
138 framework of sea level changes for Sundaland by combining variations of both glacio-eustatic  
139 and subsiding activity.

140 During the LGM, when ice sheets were at their maximum, the glacio-eustatic depression of  
141 the sea level by ~120 m had fully exposed the Sunda Shelf. Several previous studies (e.g.,  
142 Bird et al., 2005; Sathiamurthy et al., 2006; Cannon et al., 2009; Sathiamurthy et al., 2017),  
143 using sedimentological, geophysical and palynological data records from the LGM stage,  
144 reconstructed the paleogeography of Sundaland along the areas from the South China Sea and  
145 Malacca Strait to the Java Sea. The area was dominated by large fluvial drainage systems with

146 savanna and lowland evergreen vegetation in their catchment areas (Fig.1A). Sea level  
147 changes seem to play a critical role in variability of the sedimentary successions in these areas  
148 including the Jakarta Bay and the Java Sea.

149 The last marine flood that initiated ~19 ka BP had significant consequences on the  
150 remobilization of sediments of the paleolandscapes associated with the vast coastal plain,  
151 which occupied most of the present-day Java Sea. During this sea level rise, the new  
152 hydrodynamic conditions led to a reorganization of the sedimentary architecture that initiated  
153 with continental sedimentary regime to a mixed sedimentary system (i.e., both marine and  
154 continental) and then culminated in an exclusively marine-dominated stratigraphic  
155 architecture, to reach the current coastline of northern Java.

156

### 157 **3. Material and methods**

#### 158 **3.1. Geophysical data acquisition and processing**

159 Two high-resolution reflection seismic (HRRS) single channel data records were used. The  
160 first set of seismic profiles correspond to refined HRRS campaigns that were carried out in  
161 June to July 2015, covering nearly the entire Jakarta Bay. The second set of seismic profiles  
162 were obtained from the HRRS data acquisition campaign that was conducted in March 1990  
163 (unpublished report by Kurnio et al., 1991) for the Java Sea (Fig. 1B). Both seismic records  
164 were acquired by deploying a sparker system that could penetrate up to 250 ms TWTT.  
165 Cheaspeake Sonarwiz 5 software was used for processing the single channel data by  
166 completing the sea bottom track by noise attenuation, seismic signal gaining by Automatic  
167 Gain Control and User Define Gain/Attenuation, bandpass filtering through frequency  
168 selection to have a better resolution of seismic reflectors at upper layers of sub-sea bottom and  
169 seismic trace stacking by increasing the ratio of signal/noise to obtain a better quality of the

170 reflectors. The time-depth conversion for sediment unit boundaries was assumed using an  
171 internal velocity of 1600 m/s beneath the seafloor (Puchala et al., 2011; Martínez-Carreño and  
172 García-Gil, 2017). Thus, 200 m depth was reached with some approximately visible  
173 reflectors. Survey positioning was achieved with a differential global positioning system  
174 (DGPS) using CNAV 3050. The seismic reflectors were analyzed following the procedures  
175 enlisted by Mitchum and Vail (1977), Brown and Fisher (1980), Posamentier et al. (1988),  
176 Posamentier and Vail (1988), and Catuneanu (2019).

### 177 **3.2. Sediment cores**

178 Ten boreholes (BH-01–BH-10) were drilled (Figs. 1C and 2B) around the Jakarta Bay. The  
179 borehole, BH-10, has the deepest water depth (22 m below Lowest Astronomical Tide -LAT),  
180 while the others varied from 14 to 19 m water depth below LAT. Among the 10 boreholes, the  
181 drilling depth of BH-02 and BH-07 reached 150 m below the sea bed and both boreholes were  
182 located in the middle of the bay (Fig. 1C and Table 1). The other boreholes were drilled to a  
183 depth of 60 m below the seafloor. The retrieved sediment cores were used to describe the  
184 lithology, microfauna and organic matter (e.g., fragments of fossilized wood, rootlets,  
185 charcoal, etc.) to decipher the depositional environments, which were interpreted based on  
186 granulometric analyses (30 g dry samples were sieved for grain sizes 2 mm, 500  $\mu\text{m}$ , 250  $\mu\text{m}$   
187 and 63  $\mu\text{m}$ ) and microfossil analysis (using stereo zoom Zeiss Stemi SV 11) following  
188 standard procedures.

### 189 **3.3. AMS $^{14}\text{C}$ dating**

190 The selected samples for radiocarbon dating were analyzed with Accelerator Mass  
191 Spectrometry at the Radiocarbon Laboratory, University of Arizona, USA. Each age  
192 measurement was conducted on shell fragments and organic matter extracted from the cores.  
193 All radiocarbon dates are given in years before present/1950 (BP) (Smith et al., 2011; Reimer



194 et al., 2013). Radiocarbon dates with a “measured radiocarbon age” older than 46,400 yrs BP  
195 are outside the detection limits and are not calibrated; thus, these ages are shown as > 46,400  
196 yrs BP (Table. 2).

## 197 **4. Results**

### 198 **4.1. Interpretation of seismic reflection configuration patterns and seismic stratigraphy**

199 The seismic profiles were analyzed in terms of continuity, amplitude, configuration and  
200 termination of reflectors following Mitchum et al. (1977) and Catuneanu (2019). This was  
201 followed by the recognition of seismic units and description of the recognized units along  
202 with their boundaries (unit boundary - UB). The characteristics of the acoustic facies are  
203 summarized in Table 3 for the seismic units observed in the offshore zone and identified in  
204 boreholes BH-02 and BH-07.

205 To illustrate the Holocene infilling of the incised valleys from the Jakarta Bay to the Java Sea,  
206 we selected five seismic profiles that are located in the central part of the study zone.

207 In the five profiles (sparker profiles: L-42, CL-06B, L-C7, L-C8 and L-X), located at water  
208 depths ranging from 5 to 50 m, seven seismic units, i.e., U1–U7, from the base towards the  
209 top, were identified in the sedimentary infilling of the incised valleys (Fig. 4 and Table 3).

210 These units are illustrated on the selected profiles, except for Units 1, 2 and 3, which are only  
211 adequately visible on L-42. Units 1 and 2 are characterized by discontinuous reflectors with  
212 an acoustically opaque configuration.

213 Unit 1 (U1) is located in the basal part (Fig. 4A) and displays a thickness of >25 ms TWTT  
214 (>20 m). The reflectors of U1 demonstrates very poor continuity, low frequency and low  
215 amplitude (Table 3). The reflection configuration is aggrading sub-parallel with attenuated  
216 zones (acoustically opaque) as a result of subsurface gas. It should be noted that this area has

217 been shown to contain acoustically turbid zones, which are related to the presence of gas in  
218 organic-rich sediments (e.g., Schubel, 1974; Baltzer et al., 2005).

219 Unit 2 (U2) presents an acoustic thickness varying from 20 to 35 ms TWTT (~16 m to 28 m).  
220 Continuity, amplitude and frequency in seismic facies range from low to medium and very  
221 poor at some parts with acoustic turbidity (Table 3). Reflector configuration displays  
222 aggrading sub-parallel to parallel patterns associated with a shallow marine environment, such  
223 as a deltaic depositional system.

224 Unit 3 (U3) exhibits an acoustic thickness varying between 35 ms to 60 ms TWTT (~28 m to  
225 48 m). U3 is characterized by aggrading reflectors in the sedimentary prism wedging  
226 morphology systems towards the south and the north, particularly in the lower section of the  
227 seismic line L42. This seismic facies is interpreted as a deltaic depositional system.

228 Unit 4 (U4) overlies U3 (Figs. 4 and 5) and has an acoustic thickness varying between 50 ms  
229 and 70 ms TWTT (~40 m to 64 m). The reflectors show very poor to moderate continuity and  
230 the amplitude and frequency are medium (Table 3). The top of the unit is bounded by an  
231 erosional surface. The internal reflectors show corrugated reflector stacking pattern, probably  
232 due to the prevalence of superimposed subaqueous lobes within a deltaic system, and some  
233 erosional surfaces, which in turn are located at the southern and northern parts. The seismic  
234 facies could suggest that U4 comprises an alluvial plain depositional environment (Reineck  
235 and Singh, 1980; Catuneanu et al., 2009; Catuneanu, 2019).

236 Unit 5 (U5) overlies U4 with an acoustic thickness varying between 5 ms to 50 ms (~4 m to  
237 40 m) and is bounded by erosional surfaces on the top and bottom (Figs. 4 and 5). The unit  
238 extends laterally to a planar geometry. The continuity of seismic facies is very poor to poor  
239 corresponding to acoustic attenuation and demonstrates an oblique-aggrading subparallel  
240 geometry, while amplitude and frequency are low to high (Table 3). Aggrading subparallel

241 seismic reflector geometry is commonly found beside discontinuous reflectors that could  
242 indicate existing gas pockets. This unit presents a general organization of horizontal reflectors  
243 with some downlap and onlap in a few places. Using indications from the seismic facies, the  
244 depositional environment of U5 is interpreted as a delta plain with some parts containing  
245 alluvial channels and tidal flat sediments (Brown and Fisher, 1980; Reineck and Singh, 1980;  
246 Catuneanu et al., 2009; Catuneanu, 2019).

247 The next unit, U6, presents an acoustic thickness of 5 ms to 40 ms TWTT (~4 m to 32 m)  
248 (Figs. 4 and 5). This unit reveals acoustic facies that are characterized by aggrading parallel  
249 and progradation pattern of poor continuity, and low to high frequency with very low to high  
250 amplitude (Table 3). The base of U6 corresponds to a subaerial unconformity and  
251 demonstrates flat upper layers that overlie clinoform deposits in some parts (Figs. 4 and 5),  
252 which intersects U5 with a divergent filling pattern. The variation in thickness of this unit is  
253 associated with incised channels and U6 is interpreted as delta front deposits within a shallow  
254 marine setting (Reineck and Singh, 1980; Dalrymple et al., 2003; Catuneanu et al., 2009;  
255 Catuneanu, 2019).

256 Unit 7 (U7) is the most recent seismic unit which overlies U6 (Figs. 4 and 5). The seismic  
257 facies show medium to good continuity with good amplitude and medium frequency. Seismic  
258 reflector configuration is predominantly aggrading parallel (Table 3). The acoustic thickness  
259 ranges between 5 ms to 30 ms TWTT (~4 m to 24 m). The depositional environment of U7 is  
260 interpreted as a subaqueous fan delta in the south-central and eastern parts that can be  
261 associated with existing river mouths and a shoreface setting toward the north as seen in the  
262 modern bathymetric map of the study area.

## 263 **4.2. Lithofacies description and correlation from sediment cores**

264 Lithofacies description of the recognized seismic units was conducted on selected cores, i.e.,  
265 BH-02, BH-04, BH-05, BH-06, BH-07 and BH-09 (Figs. 2B and 6). It is evident from the  
266 sparker profile L-42 (Fig. 4A) that these cores represent a complete and continuous record of  
267 stratigraphic successions in units U2 to U7, and thus provide the optimal opportunity to  
268 investigate the sedimentary infilling history of the study area. U2 was recognized at a depth of  
269 130–150 m and consists of dark grey to olive grey silt and clay, and medium to dark grey  
270 very-fine to fine-grained sand and the depositional environment indicated an inner shelf  
271 setting. U3 comprises of sediments that correspond to grey clay and dark grey medium-  
272 grained sand as seen in BH-02 and BH-07 and gathering information from the seismic facies,  
273 this unit is interpreted as being deposited in a deltaic setting. The lithology of U4, as seen in  
274 cores BH-04 to BH-09, and identified at a depth of 46–100 m below the seabed, is  
275 characterized by dark grey to olive grey silt with traces of clay, medium to coarse grain  
276 greyish brown sand and silt with traces of clay that indicate a shallow marine to alluvial plain  
277 depositional environment. Core description of boreholes BH-04 and BH-09 (Fig. 6) reveal  
278 that U5 consists predominantly of greyish brown to brown sand and brownish grey silt and  
279 clay. Informed by the seismic facies and lithofacies, we interpret the depositional environment  
280 of U5 as a delta plain with some parts containing alluvial channels and tidal flat sediments.  
281 The sediments of U6, witnessed in the boreholes BH-05 and BH-07, reveal dark grey to black  
282 sand, medium to coarse grained sand and dark grey mud with some medium grain sand. The  
283 basal sequence boundary is overlain by yellowish-brown medium grain sand, reversed graded  
284 bedding, containing shell fragments, which denote a shallow marine to deltaic depositional  
285 environment. U7 occupies the stratigraphic succession between 0 to 12 m and consists of  
286 yellowish-grey clay with medium grained sand containing visually  $\pm 10\%$  of shell fragments  
287 and depositional environment is interpreted as a shallow offshore environment

#### 288 **4.3. Micropaleontological indices**

289 Microfossils were identified and described from cores BH-02, and BH-07 (Table 4).  
290 The dominant benthic foraminifera taxa (i.e., *Ammonia* spp.; *Asterorotalia* spp.) (Fig. 7 and  
291 Table 4) in U2 seem to indicate a coastal waters environment. *Ammonia tepida* is indeed  
292 known to be tolerant to continental organic matter and freshwater inputs in the southwestern  
293 Pacific region (Debenay, 2012). *Asterorotalia* spp. is a typical warm water epifaunal benthic  
294 foraminifera well represented in riverine influx dominated coastal domain (Panchang and  
295 Nigam, 2012; Saraswat et al., 2017). Microfossil barren zones are observed in U4 in both BH-  
296 02 and BH-07. A gradual increase in benthic foraminifera, especially *Elphidium* spp.,  
297 *Operculina* spp. and *Quinqueloculina* spp. is seen in the upper parts of U4 and in U5 within  
298 BH-07, while ostracods are very rare in these two units (Table 4). Similarly, in BH-02, the  
299 lack of ostracods is evident in U4 and U5, while rare occurrences of *Elphidium* spp.,  
300 *Pseudorotalia* spp. and *Quinqueloculina* spp. is noticed in upper parts of U4. U6, similar to  
301 U3, entails an abundance of various species of ostracods and benthic foraminifera and this  
302 could be indicative of a shallow marine setting (Table 4). U7 reveals the presence of some  
303 marine benthic foraminifera taxa found in modern warm marine waters of southwestern  
304 Pacific Ocean (e.g. *Dendritina* spp., *Spiroloculina* spp., Hohenegger et al., 1999; Debenay,  
305 2012). *Dendritina* spp. is indeed a full marine species frequently found abundant in regions  
306 protected from extreme hydrodynamic forcing.

307

#### 308 **4.4. Radiocarbon ages**

309 A total of 3 cores (i.e., BH-05, BH-06 and BH-07) were sampled for radiocarbon dating. The  
310 dating analysis from a sample recovered at 134.5 m depth of BH-07 and pertaining to U2  
311 revealed an age of > 49,900 ka BP.

312 In the same core,  $^{14}\text{C}$  dating results (Table 2) of samples at 77 m depth and 56.2 m depth, and  
313 within U4, presented ages of  $> 46.4$  ka BP and  $41.8 \pm 1.5$  cal ka BP, respectively.

314 The result of radiocarbon dating applied on shell materials of the sub-sample from 14.3 m  
315 below the seabed from BH-06 revealed an age of  $8461 \pm 29$  cal yrs BP (Table 2).

316 The dating applied on molluscan shell collected at 7 m depth below seafloor from BH-05  
317 returned an age of  $3,308 \pm 24$  cal yrs BP (Table 2).

## 318 **5. Discussion**

### 319 **5.1. Sequence stratigraphic framework**

320 While all the depositional units are not equally preserved in all the studied valleys, a general  
321 stratigraphic scheme can be drawn that applies over the entire zone or system.

322 The chronology of the complete succession remains speculative for Units 1, 2 and 3 except  
323 for the upper units (U4–7), wherein, the formations indicate ages ranging from the Pleistocene  
324 to Holocene. U4 that signifies the falling stage systems tract shows a first stage of incision  
325 and is characterized by alluvial deposits (Figs. 4 and 6), which indicate ages of  $> 46.4$  ka BP  
326 and  $41.8 \pm 1.5$  cal ka BP (MIS 3) (Table 2) and we interpret this sequence to be associated  
327 with the accumulation of regressional deposits following the persistent drop of relative sea  
328 level since MIS 5e. The microfossil assemblages (benthic foraminifera and ostracods) within  
329 U4 show a dramatic decline in BH-02 and BH-07 (Table 4) that further supports the  
330 interpretation of relative sea level drop and subaerial exposure of the shelf. U5 incorporates  
331 mixed fluvio-estuarine deposits that could have been emplaced initially under lowered relative  
332 sea levels, during which, regressional alluvial channel deposits continued to accumulate and  
333 sealed the first incisional features. Incision synchronously propagated across these deposits,  
334 and later as relative sea level began to gradually increase there could have been reduced  
335 incisional capacity with aggradation of sediments due to a rise in base level and some filling

336 of the incised system, and owing to these evidences, we deduce U5 to represent the lowstand  
337 systems tract. The gradual rise in sea level and estuarine sedimentation is corroborated by the  
338 increase in population of brackish and saline water favoring benthic foraminifera species such  
339 as *Elphidium* spp., *Operculina* spp. and *Quinqueloculina* spp. in BH-07. U6, demonstrating an  
340 age of  $8461 \pm 29$  cal yrs BP (Table 2) in the intermediate part of the sequence and which lies  
341 above the transgressive surface, consists of shallow marine sediments that may have been  
342 deposited during rapid transgression after ~15 ka BP, which could efficiently preserve the  
343 preceding fluvial deposits, and we posit that this unit elucidates the transgressive systems  
344 tract. Lastly, the Holocene sediments forming the hemipelagic drape of U7 that overlie the  
345 maximum flooding surface represent the highstand systems tract.

## 346 **5.2. Valley morphology**

347 As defined by the seismic data shown in figure 5 (Fig. 1B for location), the valleys run  
348 parallel to the coast and are between 1 and 10 km long. They follow a regional slope towards  
349 the shelf break and reach maximum depths of ~30 to 40 m. These valleys are increasingly  
350 wide towards the east, particularly where several valleys converge, and are linked to the  
351 confluence of fluvial channels. Indeed, there could have been high rates of sedimentation,  
352 channel flow and drainage discharge which could possibly explain the processes of alluviation  
353 and incisional dynamics that promoted the notable widening of the emerging valleys in the  
354 Java Sea (Fig. 8), that are mainly controlled by global sea level changes during the LGM  
355 (Voris et al, 2000; Hanebuth et al., 2004; Clark et al, 2009; Sar et al, 2019).

356 These valleys, filled by marine transgressive deposits (U6–shallow marine), are underlain by  
357 mixed fluviio-estuarine formations of weakly consolidated origin (U5–lowstand channel fill),  
358 the facies of which are mainly fine to medium grained.

359 The morphology of the valleys demonstrates generally a flat bottom and markedly steep edges  
360 (Fig. 5).

361 The morphology with a flat bottom and marked edge can be explained by the lithological  
362 nature of the incised unit (U5), consisting of weakly consolidated and easily remobilized  
363 alluvial plain deposits, and conversely as a zone where the potential for incision is very low  
364 given the low to medium slopes in a region very far from the continental slope (Fig. 8A).  
365 The incision depths of ~8 m to 32 m, (Fig. 5) are of the same order as those documented from  
366 other parts of the world, for example, on the platforms of the American east coast (Thomas  
367 and Anderson, 1994; Foyle and Oertel, 1997), the Bay of Biscay (Lericolais et al., 2001;  
368 Chaumillon et al., 2008; Chaumillon et al. 2010; Menier et al., 2010; Estournès et al., 2012;  
369 Menier et al., 2014; Martínez-Carreño and García-Gil, 2017), the Mediterranean (Tesson et  
370 al., 2010; Tesson et al., 2015), India (Dubey et al., 2019) and also in Southeast Asia  
371 (Hanebuth, et al., 2009; Puchala et al., 2011; Alqahtani, et al., 2015; Wang et al., 2020;  
372 Horozal et al., 2021).

### 373 **5.3. Depositional evolution**

374 The main stratigraphic units recognized across the study area are composed of continental  
375 formations (U4 and U5) that transitions upward to shallow marine deposits (U6 and U7). This  
376 interpretation is also confirmed by the succession of fossil foraminifera faunas, from taxa that  
377 are indicative of environments under continental influence (*e.g. Asterorotalia* spp.) to those  
378 that are indicators of shallow coastal waters (*e.g. Dendritina* spp., *Spiroloculina* spp.,  
379 *Operculina* spp.) (Fig. 7 and Table 4). The core and the major parts of the valley fills are  
380 composed of alluvial deposits (U5) and shallow marine deposits (U6 and U7), and the vertical  
381 facies succession is predominantly deposited within a transgressive setting.

382 In our proposed model of valley morphogenesis, the supposed thalweg, which overlays the  
383 erosional surface UB-4, is dated at 41800 +/- 1500 cal. age BP, which corresponds to the last  
384 and deepest incision (pre-LGM incision), and therefore, the overlaying fluvial deposits (U5)  
385 could be younger than 25 ka. Based on deductions implied in previous studies (*e.g.*,



386 Posamentier and Allen, 1999; Posamentier, 2001), the alluvial channels more than likely  
387 formed when the shelf was not fully subaerially exposed and the lowstand fluvial system was  
388 incapable of substantially efficient downcutting, both laterally and vertically.

389 On the seismic records (Fig. 3B and Table 3) U4 seem to illustrate an irregular and oblique  
390 aggrading subparallel or wavy reflector geometry and we interpret it as interfluves or bars,  
391 dominated by sandy to silt-argillaceous facies established during the marine isotopic stage 3  
392 (Fig. 9).

393 Unit 5 is interpreted to consist of lowstand channel fill deposits that accumulated during  
394 periods of significant drops in sea level but the majority during the post lowstand system tract  
395 (LST), which was lower than present-day in this zone (Fig. 9). Our results clearly highlight  
396 the occurrence of alluvial channel deposits and nearshore tidal flat sediments that are  
397 explicitly indicative of a shift from a relatively sand-rich lowstand system to a clay-rich  
398 nearshore sediment as mention in Table 4. Gathering consensus from the global and Sunda  
399 shelf sea level curves (Fig. 9), the transition from a fluvial to a shallow marine setting in our  
400 data could correspond to the post-LGM abrupt and rapid sea level rise induced by  
401 deglaciation. Furthermore, our inference of an abrupt and rapid rise in sea level is congruent  
402 with previous findings (Hanebuth et al., 2000) of an accelerated increase in eustatic levels in  
403 the northern Sunda Shelf during the MWP 1A (meltwater pulse) event that commenced at  
404 ~14.7 ka and terminated before ~13.8 ka, including an abrupt rise of up to ~16 m within a  
405 span of 300 years that occurred between 14.6–14.3 ka cal BP (Hanebuth et al., 2000).

406 Unit 6, dated at ~8461 +/- 29 cal. age BP, which mainly rests above Unit 5, is interpreted as  
407 deposited in the course of the last sea level rise over the area (Fig. 8). As the fluvial valleys  
408 were flooded by the rising sea levels, sediment supply could not keep pace with the increase  
409 of accommodation space, and this would explain the aggrading nature of Unit 6. The very  
410 homogeneous structure of Unit 6 and the inferred fine-grained sedimentation would point to a

411 wave-dominated bay (Dalrymple et al., 1994). While there is an inexistence of sandy barriers  
412 in the seismic record, the Java Sea seems to be a sector that was very calm, favoring low-  
413 energy sedimentation comparable to that in estuarine central basins (lagoonal basins). Further  
414 expanding on our sedimentological and seismic data, we favor the interpretation of very calm  
415 and low-energy conditions in the Java Sea during the deposition of Unit 6. We base this on an  
416 additional line of evidence, viz. the preservation of Unit 5 could be plausible only under rapid  
417 transgression and placid hydrodynamic environments. This can effectively weaken potential  
418 erosional processes, given that ubiquitously, the efficient preservation of lowstand fluvial  
419 deposits, subsequent to erosion during transgression and reworking by inclement  
420 hydrodynamic conditions, would be, at best, in patches (Allen, 1991; Allen and Posamentier,  
421 1993; Posamentier, 2001).

422 Unit 7 is interpreted as offshore muds aggrading above the estuarine valley fills as the first  
423 succession overlaying UB-6. It rests above the maximum flooding surface that truncates all  
424 the units below (Figs. 4 and 10). The unit is dated at  $\sim 3308 \pm 24$  yr BP, and is composed of  
425 Holocene-age hemipelagic drape. U7 was emplaced during a full transgression over the area,  
426 inasmuch as it overlaps most of the valley interfluves.

## 427 **6. Conclusions**

428 Two remarkable incisions are identified in the Java Sea shelf. The first incision occurred  
429 during the sea level drop of the marine isotopic stage 3, which was later sealed by  
430 lowstand alluvial channel deposits. These deposits were re-incised during the LGM,  
431 creating the second incisional surface. This discontinuity does not intersect the Upper  
432 Pleistocene incision, indicating a relatively low incision potential, in a context of rapid sea  
433 level rise within very sheltered hydrodynamic conditions.

434 The incised valleys demonstrate a wide and flat bottom morphology along with very steep  
435 edges owing to low velocity channel flow and shallow paleo-topographic gradients. The

436 sedimentary infill of the incised valleys indicates the continent-offshore extension of the  
437 paleodeltaic system, complete with variable facies characteristics and variable rates of  
438 deposition. Influences of regional slope and hydrodynamics are recognized to have  
439 exercised control over the spatial distribution of facies types as well as grain sizes of the  
440 facies types.

441 Prevalence of major river systems that drained the Sundaland Craton that advanced over  
442 former offshore regions during LGM created an extensive incised valley and associated  
443 geomorphic-sedimentary infill.

#### 444 **Author Contributions**

445 Author Contributions: Conceptualisation: F.N., D.M., M.M., H. and C.E.; methodology: F.N.,  
446 D.M., R.K. and M.S.; field investigation: F.N. and I.K.; manuscript preparation: F.N., D.M.,  
447 M.M., M.R. and H.; review and editing: F.N., D.M., M.M., M.R., M.S. and C.E.; figures:  
448 D.M., M.M., F.N., and C.E.; microfossil analysis: F.N. and K.T.D.

#### 449 **Acknowledgements**

450 The field activities were fully supported by the Ministry of Public Works and Housing, the  
451 Republic of Indonesia, under the grant bearing the contract number HK.02.03/PPK-  
452 PP/SBBWSCC/1311.2 and also by the Ministry of Energy and Mineral Resources, the  
453 Republic of Indonesia, under the contract number P.P.G.L. G.F. 030.90. We also  
454 acknowledge the Embassy of France in the Republic of Indonesia and M. Jean-Charles  
455 BERTHONNET for providing the funding for the AMS analysis through the ‘Programme  
456 Science and Impact’ (March 2017) initiative. M.M. was supported by the ISblue project,  
457 Interdisciplinary Graduate School for the blue planet (ANR-17-EURE-0015) and by a grant

458 from the French Government under the program “Investissements d’Avenir”. We express our  
459 gratitude to Ir. Duddy Ranawijaya for significantly contributing to improve the manuscript.

460

## 461 **References**

462 Abidin, H.Z., Andreas, H., Djaja, R., Darmawan, D., Gamal, M., 2008. Land subsidence  
463 characteristics of Jakarta between 1997 and 2005, as estimated using GPS surveys.  
464 GPS Solutions 12, 23-32.

465 Abidin, H.Z., Andreas, H., Gumilar, I., Sidiq, T.P., Fukuda, Y., 2013. On the roles of  
466 geospatial information for risk assessment of land subsidence in urban areas of  
467 Indonesia. In: Zlatanova, S., Peters, R., Dilo, A., Scholten, H. (eds.), Intelligent  
468 Systems for Crisis Management. Lecture Notes in Geoinformation and Cartography.  
469 Springer, Berlin, Heidelberg, 277-288.

470 Abidin, H.Z., Andreas, H., Gumilar, I., Brinkman, J.J., 2015. Study on the risk and impacts of  
471 land subsidence in Jakarta. Proceedings of the International Association of  
472 Hydrological Sciences 372, 115–120.

473 Adams, J., Maslin, M., Thomas, E., 1999. Sudden climate transitions during the Quaternary.  
474 Progress in Physical Geography 23(1), 1-36.

475 Adriansyah, A., McMechan, G.A., 2002. Case History, Analysis and Interpretation of seismic  
476 data from thin reservoirs: Northwest Java Basin, Indonesia. Journal of Geophysics 67  
477 (1), 14-26.

478 Allen, G.P., 1991. Sedimentary processes and facies in the Gironde estuary: A Recent model  
479 for macrotidal estuarine systems. In: Smith, D.G., Reinson, G.E., Zaitlin, B.A. and  
480 Rahmani, R.A. (eds.), Clastic tidal sedimentology. Canadian Society of Petroleum  
481 Geologists Memoir 16, 29–40.

482 Allen, G.P., and Posamentier, H.W., 1993, Sequence stratigraphy and facies model of an  
483 incised valley fill: the Gironde Estuary, France. *Journal of Sedimentary Petrology* 63,  
484 378–391.

485 Allen, G.P. and Posamentier, H.W. 1994. Transgressive facies and sequence architecture in  
486 mixed tide- and wave-dominated incised valleys: example from the Gironde estuary.  
487 France. In: Dalrymple, R.W., Zaitlin, B.A. and Boyd, R. (eds.), *Incised valley*  
488 *systems: origin and sedimentary sequences*. Society of Economic Paleontologists and  
489 Mineralogists, Special Publications 51, 225-240.

490 Alqahtani, F.A., Johnson, H.D., Jackson, C.A.-L, Som, M.R.B., 2015. Nature, origin and  
491 evolution of a Late Pleistocene incised valley-fill, Sunda Shelf, Southeast Asia.  
492 *Sedimentology* 62, 1198–1232.

493 Baltzer, A., Tessier, B., Nouze, H., Bates, R., Moore, C., Menier, D., 2005. Seistec seismic  
494 profiles: A tool to differentiate gas signatures. *Marine Geophysical Researches* 26,  
495 235-245.

496 Bird, M.I., Taylor, D., Hunt, C., 2005. Palaeoenvironments of insular Southeast Asia during  
497 the Last Glacial Period: a savana corridor in Sundaland? *Quaternary Science Reviews*  
498 24, 2228-2242.

499 Brown, L.F. and Fisher, W.L., 1980. Seismic-stratigraphic interpretation of depositional  
500 systems and its role in petroleum exploration. AAPG Continuing Education Course  
501 Notes Series 16, 1-181.

502 Catuneanu, O., Abreu, V., Bhattacharya, J.P., Blum, M.D., Dalrymple, R.W., Eriksson, P.G.,  
503 Fielding, C.R., Fisher, W.L., Galloway, W.E., Gibling, M.R., Giles, K.A., Holbrook,  
504 J.M., Jordan, R., Kendall, C.G.St.C., Macurda, B., Martinsen, O.J., Miall, A.D., Neal,  
505 J.E., Nummedal, D., Pomar, L., Posamentier, H.W., Pratt, B.R., Sarg, J.F., Shanley,

506 K.W., Steel, R.J., Strasser, A., Tucker, M.E., Winker, C., 2009. Towards the  
507 standardization of sequence stratigraphy. *Earth-Science Reviews* 92, 1-33.

508 Catuneanu, O., 2019. Scale in sequence stratigraphy. *Marine and Petroleum Geology* 106,  
509 128–159.

510 Chaumillon, E., Proust, J.N., Menier, D., Weber, N., 2008. Incised-valleys morphologies and  
511 sedimentary-fills within the inner shelf of the Bay of Biscay (France): A synthesis.  
512 *Journal of Marine Systems* 72, 383-396.

513 Chaumillon, E., Tessier, B., Reynaud, J.Y., 2010. Stratigraphic records and variability of  
514 incised valleys and estuaries along French coasts. *Bulletin de la Société Géologique de*  
515 *France* 181, 75-85.

516 Chaussard, E., Amelung, F., Abidin, H., Hong, S-H., 2013. Sinking cities in Indonesia: ALOS  
517 PALSAR detects rapid subsidence due to ground water and gas extraction. *Remote*  
518 *Sensing of Environment* 128, 150-161.

519 Clark, P.U., Dyke, A.S., Shakun, J.D., Carlson, A.E., Clark, J., Wohlfarth, B., Mitrovica, J.X.,  
520 Hostetler, S.W., McCabe, A.M., 2009. The Last Glacial Maximum. *Science* 325, 710-  
521 714.

522 Dalrymple R.W., Boyd, R., Zaitlin, B.A., 1994. History of research, types and internal  
523 organization of incised-valley systems: introduction to the volume. In: Dalrymple,  
524 R.W., Boyd, R.J., Zaitlin, B.A. (eds.), *Incised-valley systems: origin and sedimentary*  
525 *sequences*. Society for Sedimentary Geology special publication 51, 5–12.

526 Dalrymple, R.W., Baker, E.K., Harris, P.T., Hughes, M.G., 2003. Sedimentology and  
527 stratigraphy of a tide-dominated foreland-basin delta (Fly River, Papua New Guinea).  
528 In: Sidi, F.H., Nummedal, D., Imbert, P., Darman, H., Posamentier, H.W. (eds.),

529 Tropical Deltas of Southeast Asia-sedimentology, Stratigraphy, and Petroleum  
530 Geology. SEPM 76, 147-173.

531 Darman, H. and Sidi, F.H., 2000; An outline of the geology of Indonesia. Indonesian  
532 Association of Geologists, IAGI, Jakarta, 192 pp.

533 Dubey, K.M., Chaubey, A.K., Mahale, V.P., Karisiddaiah, S.M., 2019. Buried channels  
534 provide keys to infer Quaternary stratigraphic and paleo-environmental changes: A  
535 case study from the west coast of India. Geoscience Frontiers 10, 1577-1595.

536 Durand, J.R. and Petit, D., 1995. The Java Sea environment. in: BIODYNEX: Biology,  
537 Dynamics, Exploitation of the small pelagic fishes in the Java Sea. Potier, M. and  
538 Nurhakim, S. (eds.), Java Sea Pelagic Fishery Assessment Project. AARD/ORSTOM,  
539 14-38.

540 Elias, S.A., 2013. The Quaternary. Reference Module in Earth Systems and Environmental  
541 Science, Elsevier. DOI: <https://doi.org/10.1016/B978-0-12-409548-9.05350-1>.

542 Emery, K.O., Uchupi, E., Sunderland, J., Uktolseja, H.L, Young, E.M., 1972. Geological  
543 structure and some water characteristics of the Java Sea and adjacent continental shelf.  
544 CCOP Technical Bulletin 6, 197-221.

545 Estournès, G., Menier, D., Guillocheau, F., Le Roy, P., Paquet, F. and Goubert, E., 2012. The  
546 paleo-Etel River incised valley on the Southern Brittany inner shelf (Atlantic coast,  
547 France): Preservation of Holocene transgression within the remnant of a middle  
548 Pleistocene incision? Marine Geology 329-331, 75–92.

549 Fielding, C.R., Trueman, J.D., Alexander, J., 2005. Sharp-based, flood dominated mouth bar  
550 sands from the Burdekin River Delta of northeastern Australia: extending the spectrum

551 of mouth-bar facies, geometry, and stacking patterns. *Journal of Sedimentary Research*  
552 75, 55–66.

553 Foyle, A.M. and Oertel, G.F., 1997. Transgressive systems tract development and incised-  
554 valley fills within a Quaternary estuary shelf system: Virginia inner shelf, USA.  
555 *Marine Geology* 137, 227–249.

556 Genia, A.N., Nugroho, A.S., Olugbenda, J.O., 2007. Introduction to Java Sea. *Oceanography*.  
557 Stavanger, University of Stavanger.

558 Gornitz, V., 2021. Timescales of climate change. In: Alderton, D., Elias, S.A. (Eds.),  
559 *Encyclopedia of Geology* (second edition). Academic Press, pp. 318-327.

560 Green, A.N., 2009. Palaeo-drainage, incised valley fills and transgressive systems tract  
561 sedimentation of the northern KwaZulu-Natal continental shelf, South Africa, SW  
562 Indian Ocean. *Marine Geology* 263, 46-63.

563 Haberland, C., Bohm, M., Asch, G., 2014. Accretionary nature of the crust of Central and  
564 East Java (Indonesia) revealed by local earthquake travel-time tomography. *Journal of*  
565 *Asian Earth Sciences* 96, 287–295.

566 Hamilton, W., 1979. *Tectonics of the Indonesian region*. United State of Geological Survey,  
567 Washington, 1078 pp.

568 Hanebuth, T., Stattegger, K., Grootes, P.M., 2000. Rapid flooding of the Sunda Shelf: A Late-  
569 Glacial sea-level record. *Science* 288, 1033-1035.

570 Hanebuth, T.J.J., Stattegger, K., Bojanowski, A., 2009. Termination of the last glacial  
571 maximum sea-level lowstand: the Sunda-Shelf data revisited. *Global and Planetary*  
572 *Change* 66, 76-84.



573 Hanebuth, T.J.J, Voris, H.K, Yokoyama, Y., Saito, Y., Okuno, J., 2011. Formation and fate of  
574 sedimentary depocentres on Southeast Asia's Sunda Shelf over the past sea-level cycle  
575 and biogeographic implications. *Earth-Science Reviews* 104, 92-110

576 Heaney, L.R., 1991. A Synopsis of Climatic and Vegetational Change in Southeast Asia.  
577 *Climatic Change* 19, 53–61.

578 Horozal, S., Chae, S., Seo, J.M., Lee, S.M., Han, H.S., Cukur, D., Kim, D.G., Son, J.H., 2021.  
579 Quaternary evolution of the southeastern Korean continental shelf, East Sea: Paleo-  
580 incised valley and channel systems. *Marine and Petroleum Geology* 128, 105011.

581 Husson, L., Boucher, F.C., Sarr, A.-C., Sepulchre, P., Cahyarini, S.Y., 2019. Evidence of  
582 Sundaland's subsidence requires revisiting its biography. *Journal of Biogeography* 47,  
583 843-853.

584 Irwanto, D., 2019. Sundaland: Tracing the cradle of civilizations. *Indonesia Hydro Media*,  
585 386 pp.

586 Kong, X.H., Liu, J., Du, Y.S., Wen, C., Xu, G., 2011. Seismic geomorphology of buried  
587 channel systems in the western South Huanghai Sea: retrodiction for  
588 paleoenvironments. *Acta Oceanologica Sinica* 30, 47-58.

589 Kurnio, H., Ilahude, D., Prawirasastra, R., Suprijadi, Kuntoro and Arifin, L., 1991. A report of  
590 marine geological and geophysical investigation of the Java Sea (Map sheet 1210).  
591 Unpublished report.

592 Lericolais, G., Berne, S., Fenies, H., 2001. Seaward pinching out and internal stratigraphy of  
593 the Gironde incised valley on the shelf (Bay of Biscay). *Marine Geology* 175, 183-  
594 197.

- 595 Marliyani, G.I., 2016. Neotectonics of Java, Indonesia: Crustal Deformation in the Overriding  
596 Plate of an Orthogonal Subduction System. PhD Thesis, Arizona University, 371pp.
- 597 Martínez-Carreño, N. and García-Gil, S., 2017. Reinterpretation of the Quaternary  
598 sedimentary infill of the Ría de Vigo, NW Iberian Peninsula, as a compound incised  
599 valley. *Journal of Quaternary Science Reviews* 173, 124-144.
- 600 Menier, D., Reynaud, J.Y., Proust, J-N., Guillocheau, F., Guennoc, P., Tessier, B., Bonnet, S.,  
601 Goubert, E., 2006. Basement control on shaping and infilling of valleys incised at the  
602 southern coast of Brittany, France. *S.E.P.M. Society for Sedimentary Geology, Special*  
603 *Publication* 85, 37-55.
- 604 Menier, D., Tessier, B., Proust, J.N., Baltzer, A., Sorrel, P., Traini, C., 2010. The Holocene  
605 transgression as recorded by incised-valley infilling in a rocky coast context with low  
606 sediment supply (southern Brittany, western France). *Bulletin de la Société*  
607 *Géologique de France* 181 (2), 115–128.
- 608 Menier, D., Augris, C., Briend, C., 2014. Les réseaux fluviatiles anciens du plateau  
609 continental de Bretagne Sud. Ed. QUAE, 104 p.
- 610 Metcalfe, I., 2011. Tectonic framework and Phanerozoic evolution of Sundaland. *Gondwana*  
611 *Research*, 19(1), pp.3-21.
- 612 Mitchum, R.M. and Vail, P.R., 1977. Seismic stratigraphy and global changes of sea-level,  
613 part 7. Seismic stratigraphic interpretation procedure. *AAPG Memoir* 26, 135-143.
- 614 Moreira, D.A., Gomes, M.P. & Vital, H., 2019. Shallow sedimentation of Natal shelf and  
615 coastal erosion implications, NE Brazil. *Geo-Marine Letters* 40, 843-851.
- 616 Nordfjord, S., Goff, J.A., Austin, J.A., Gulick, S.P.S., 2006. Seismic facies of incised-valley  
617 fills, New Jersey continental shelf: implications for erosion and preservation processes

618 acting during latest Pleistocene–Holocene transgression. *Journal of Sedimentary*  
619 *Research* 76, 1284-1303.

620 Patmosukismo, S. and Yahya, I., 1974. The basement configuration of the Northwest Java  
621 area. *Proceeding of the Third Annual Convention, Indonesian Petroleum Association,*  
622 129-152.

623 Posamentier, H.W., 2001. Lowstand Alluvial Bypass Systems: Incised vs. Unincised. *AAPG*  
624 *Bulletin* 85 (10), 1771–1793.

625 Posamentier, H.W. and Allen, G.P., 1999. Siliciclastic sequence stratigraphy: concepts and  
626 applications. *SEPM Concepts in Sedimentology and Paleontology* 9, 210 p.

627 Puchala, R.J., Porębski, S.J., Śliwiński, W.R., August, C.J., 2011. Pleistocene to Holocene  
628 transition in the central basin of the Gulf of Thailand, based on geoacoustic survey and  
629 radiocarbon ages. *Marine Geology* 288, 103-111.

630 Reineck, H.E., Singh, I.B., 1980. *Depositional Sedimentary Environments*, second ed.  
631 Springer-Verlag, New York, 430 pp.

632 Sarr, A.-C., Husson, L., Sepulchre, P., Pastier, A.-M., Pedoja, K., Elliot, M., Arias-Ruiz, C.,  
633 Solihuddin, T., Aribowo, S., Susilohadi, 2019. Subsiding Sundaland. *Geology* 47 (2),  
634 119-122.

635 Sathiamurthy, E., Voris, H.K., 2006. *Maps of Holocene Sea Level Transgression and*  
636 *Submerged Lakes on the Sunda Shelf. The Natural History of Chulalongkorn*  
637 *University, Supplement 2:1-43.*

638 Sathiamurthy, E., Rahman, M.M., 2017. Late Quaternary paleo fluvial system research of  
639 Sunda Shelf: A review. *Bulletin of the Geological Society of Malaysia* 64, 81-92.

640 Shennan, I., 2018. Sea Level Studies – Overview. Reference Module in Earth Systems and  
641 Environmental Sciences, Elsevier. [https://doi.org/10.1016/B978-0-12-409548-](https://doi.org/10.1016/B978-0-12-409548-9.11063-2)  
642 [9.11063-2](https://doi.org/10.1016/B978-0-12-409548-9.11063-2).

643 Schubel, J.R., 1974. Gas bubbles and the acoustically impenetrable, or turbid, character of  
644 some estuarine sediments. In: Kaplan, I.R. (Ed.), *Marine Science*, Vol. 3. Plenum Press, New  
645 York, pp. 275–298.

646 Smith, D.E., Harrison, S., Firth, C.R., Jordan, J.T., 2011. The early Holocene sea level rise.  
647 *Quaternary Science Reviews* 30, 1846-1860.

648 Suter, J.R., Berryhill, H.L., Penland, S., 1987. Late Quaternary sea level fluctuations and  
649 depositional sequences, Southwest Louisiana continental shelf. In: Nummedal, D.,  
650 Pilkey, O.H., Howard, S.D. (Eds.), *Sea Level Fluctuation and Coastal Evolution*.  
651 *SEPM Special Publication* 41, pp. 199 – 219.

652 Suyanto, F.X. and Sumantri, Y.R., 1977, Preliminary study on the Tertiary depositional  
653 patterns of Java: 6th Annual Convention Proceedings Indonesian Petroleum  
654 Association 2, 183–213.

655 Tesson, M., Posamentier, H.W., Gensous, B., 2000. Stratigraphic organization of Late  
656 Pleistocene deposits of the western part of the Golfe du Lion Shelf (Langedoc Shelf),  
657 western Mediterranean Sea, using high-resolution seismic and core data. *American*  
658 *Association of Petroleum Geologists Bulletin* 84, 119–150.

659 Tesson, M., Labaune, C., Gensous, B., Delhaye-Prat, V., 2010. Quaternary compound incised  
660 valleys of the Roussillon coast (SE France): correlation of seismic data with core data  
661 *Bulletin de la Société Géologique de France* 181 (2), 183–196.

662 Tesson, M., Posamentier, H.W., Gensous, B., 2015. Compound incised-valley  
663 characterization by high-resolution seismics in a wave-dominated setting: Example of  
664 the Aude and Orb rivers, Languedoc inner shelf, Gulf of Lion, France. *Marine*  
665 *Geology* 367, 1-21.

666 Thomas, M.A. and Anderson, J.B., 1994. Sea-level controls on the facies architecture of the  
667 Trinity/Sabine incised-valley system, Texas continental shelf, in Dalrymple, R.W.,  
668 Boyd, R., and Zaitlin, B.A., *Incised-Valley Systems: Origin and Sedimentary*  
669 *Sequences: SEPM, Special Publication 51*, 63–82.

670 Twarog, M.R., Culver, S.J., Mallinson, D.J., Leorri, E., Donovan, B., Harrison, E.I., Hindes,  
671 H., Reed, D., Horsman, E., Shazili, N.A.M., Parham, P.R., 2021. Depositional  
672 environments and sequence stratigraphy of post-last glacial maximum incised valley-  
673 fill, Malay Basin, northern Sunda Shelf. *Marine Geology* 436, 106457.

674 Voris, H.K., 2000. Maps of Pleistocene sea levels in Southeast Asia: shorelines, river systems  
675 and time durations. *Journal of Biogeography* 27, 1153-1167.

676 Wang, R., Colomera, L., Nigel, P., Mountey, P., 2020. Quantitative analysis of stratigraphic  
677 architecture of incised-valley fills: A global comparison of Quaternary systems. *Earth*  
678 *Science Reviews* 200, 102988.

679 Zahirovic, S., Flament, N., Muller, R., Seton, M., Gurnis, M., 2016. Large fluctuations of  
680 shallow seas in low-lying Southeast Asia driven by mantle flow. *Geochemistry,*  
681 *Geophysics, Geosystems* 17 (9), 3589-3607.

682

683 **Caption Figures**

684 **Figure 1. A:** Map showing the spatial distribution and type of vegetation cover in Sundaland  
685 during the LGM. Figure adapted from Heaney (1991), Voris (2000) and Bird et al. (2005). **B:**  
686 Location of seismic lines in the Java Sea and also shown are the bathymetry contours. **C:**  
687 Location of seismic lines and boreholes used in this study from the Jakarta Bay.

688 **Figure 2. A.** Map of the Java Sea seafloor sediments. **B.** Map of seafloor sediments of the  
689 Jakarta Bay (Harkin, et al., 2004) and geology of the Jakarta-Tangerang area.

690 **Figure 3.** Map showing the bathymetry and morphobathymetric features of the Java Sea and  
691 the Indian Ocean. Also shown is the drainage basins and the fluvial network of Java. Note the  
692 large drainage basins in the north and the smaller basins in the south. The southeastern limit  
693 of the Sunda Shelf is visible at the ~110 m

694 **Figure 4. A:** Sparker 2D High Resolution Seismic profile L-42. The profile passes through  
695 cores BH-02 and BH-07, south to north in the Jakarta Bay. Vertical scale in two-way travel  
696 time in seconds (TWTs). The scale in meters is established for sediments with P-wave  
697 velocity of 1600 m/sec. **B:** Sparker 2D High Resolution Seismic profile CL-06, west to east in  
698 the Jakarta Bay. Vertical scale in two-way travel time in seconds (TWTs). The scale in meters  
699 is established for sediments with P-wave velocity of 1600 m/sec.

700 **Figure 5.** Sparker 2D High Resolution Seismic profiles C-8, C-7 and C-X. The profile C-8 is  
701 located in. Vertical scale is in two-way travel time in seconds (s TWT). The scale is in meters  
702 and is established for sediments with P-wave velocity of 1600 m/sec.

703 **Figure 6.** Stratigraphic correlation of the facies types recognized in the sediment cores and  
704 interpretation of corresponding depositional environments. Also shown are the stratigraphic  
705 positions of samples used for AMS <sup>14</sup>C dating.

706 **Figure 7.** Microfossil assemblages that aided in the interpretation of the depositional  
707 environments of the sediments. Benthic foraminifera: 1. *Asterorotalia*; 2. *Operculina*; 3 & 7

708 *Pseudorotalia*; 4. *Quinqueloculina*; 5 & 6. *Elphidium*; 8-10. *Ammonia yabei*. Ostracoda: 11.  
709 *Phlyctenophora*; 12. *Neocytheretta*; 13. *Loxoconcha*; 14. *Keijella*; 15. *Neomonoceratina*; 16  
710 *Hemicytheridea*

711 **Figure 8. A:** Reconstructed paleochannel network of the offshore Java Sea based on High  
712 Resolution seismic profiles (location of all lines shown in 1B). **B:** Time slice from the north  
713 of the study area at ~72 m subsea showing the principal trunk incised valley and associated  
714 components of the fluvial system such as incised dendritic tributary valleys, scroll bars and  
715 abandoned meander loops. Figure modified from Posamentier (2001).

716 **Figure 9.** Regime diagram showing the global eustatic sea level and Sunda shelf sea level  
717 curve for the past 125 ka and 20 ka, respectively, along with timing of the major Marine  
718 Isotopic Stages (1–5) and the Last Glacial Maximum. Sunda shelf sea-level curve is adapted  
719 from Twarog et al. (2021). Red stars indicate the calibrated ages of sedimentary units (shown  
720 with white circles and U7–4) from <sup>14</sup>C radiocarbon dating of shells, shell fragments and  
721 sediments.

722 **Figure 10. A:** Present-day sedimentary architecture of the northern Java Sea. **B:** Schematic  
723 depiction of the evolution of incised valley fill in Java Sea, modified from Posamentier  
724 (2001). It shows from the time of maximum sea level lowstand, (A) sedimentation was  
725 characterized by fluvial deposition, (B) followed by rapid transgression and filling by traction  
726 and hemipelagic sedimentation, and finally, (C) the time of sea-level highstand and deposition  
727 of hemipelagic drape over the entire area.

728

## 729 **List of Tables**

730 **Table 1.** Locations, water depth and lengths of sediment cores recovered from the the Jakarta  
731 Bay and analysed in this study

732 **Table 2.** AMS <sup>14</sup>C dating of shells, shell fragments and sediments retrieved from the cores

733 **Table 3.** Characteristics of acoustic facies and seismic units and their interpretation in terms

734 of depositional environments.

735 **Table 4.** Microfossil abundances in BH-02 and BH-07

736

737

738

739

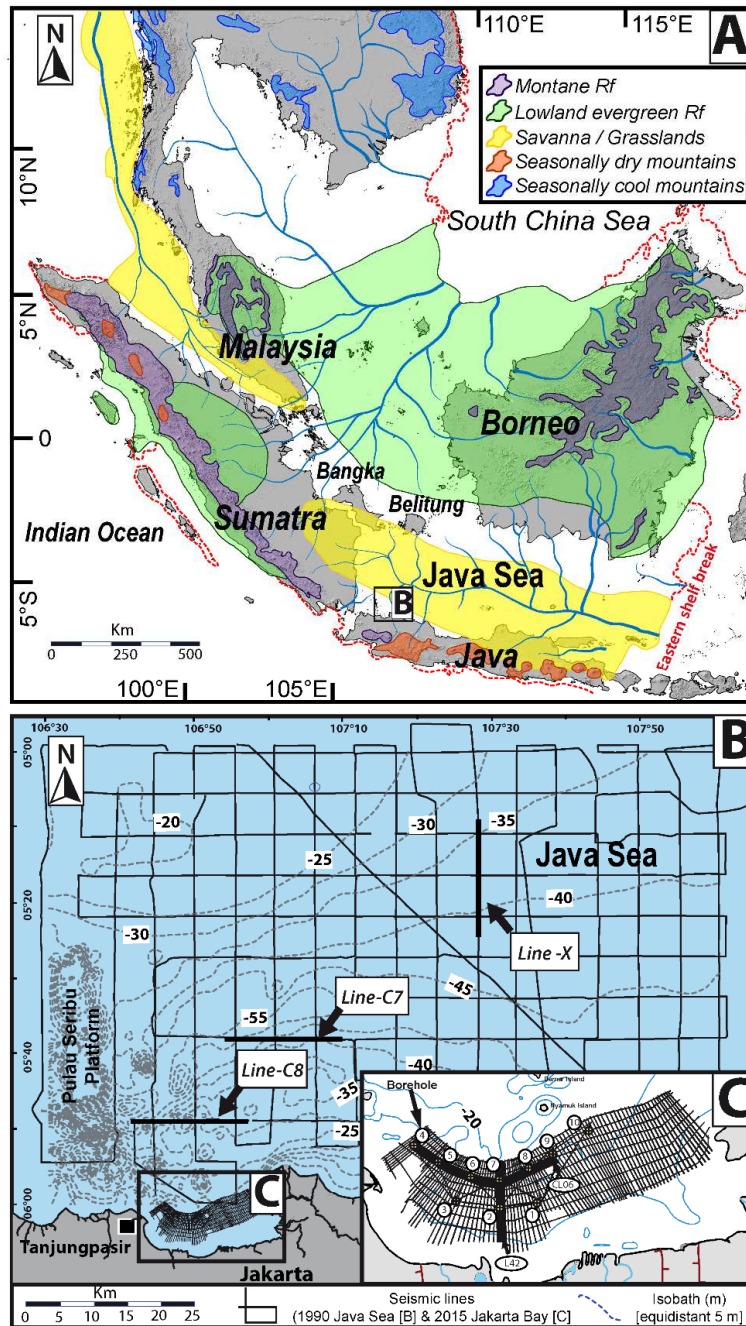
740

741

742

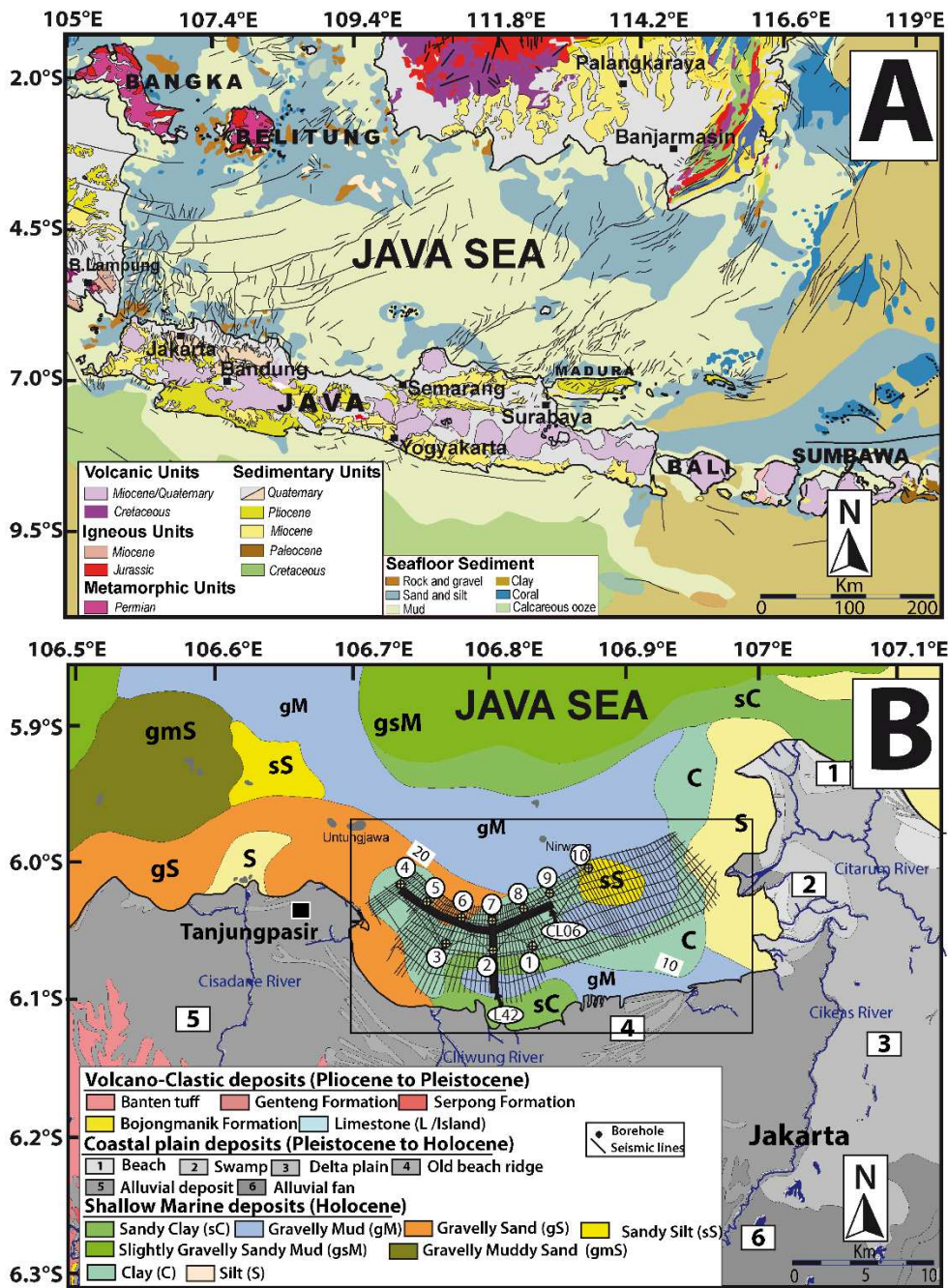
743 **Figures**



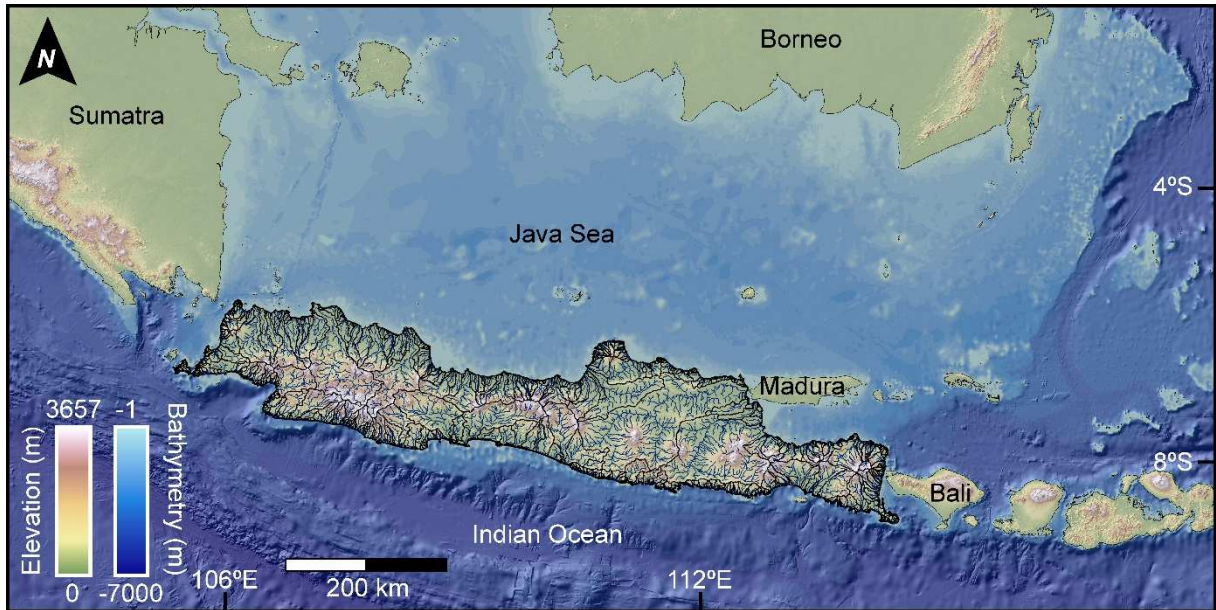


744

745 **Figure 1. A:** Map showing the spatial distribution and type of vegetation cover in Sundaland  
 746 during the LGM and red dashed line shows the approximate spatial extent of exposed  
 747 landmass of Sundaland during the LGM. Figure adapted from Heaney (1991), Voris (2000)  
 748 and Bird et al. (2005). **B:** Location of seismic lines in the Java Sea and also shown are the  
 749 bathymetry contours. **C:** Location of seismic lines and boreholes used in this study from the  
 750 Jakarta Bay.

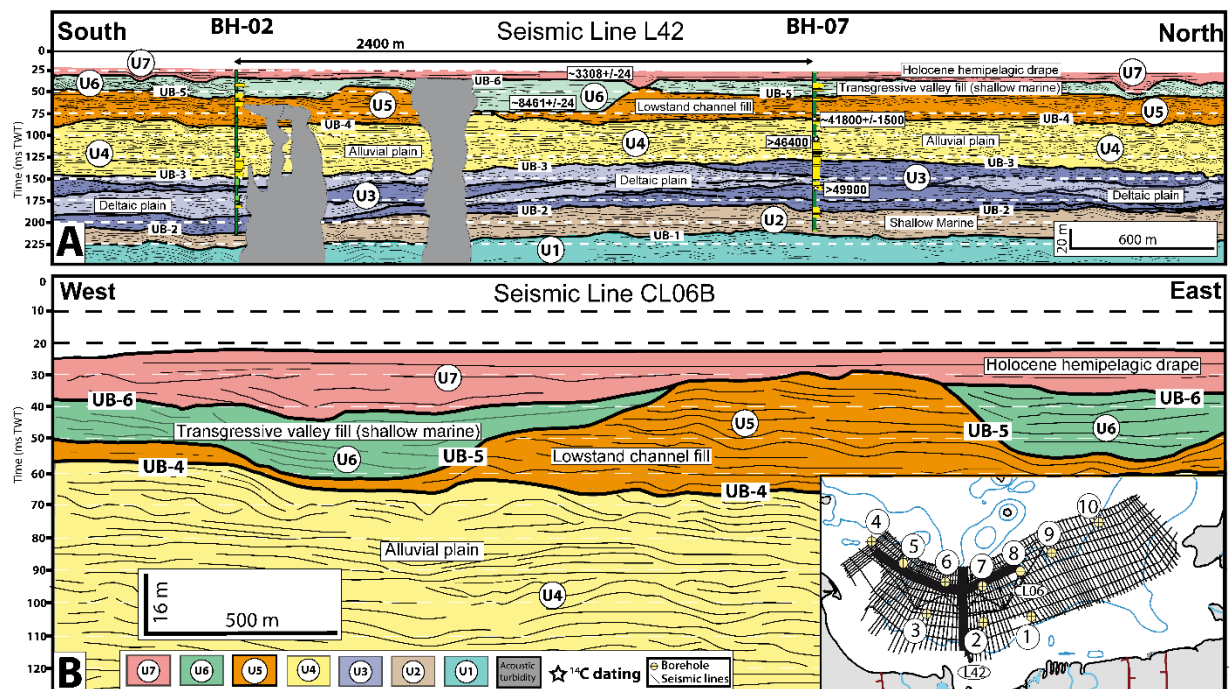


753 **Figure 2.** A. Map of the Java Sea seafloor sediments. B. Map of seafloor sediments of the  
 754 Jakarta Bay (Harkin, et al., 2004) and geology of the Jakarta-Tangerang area.



756

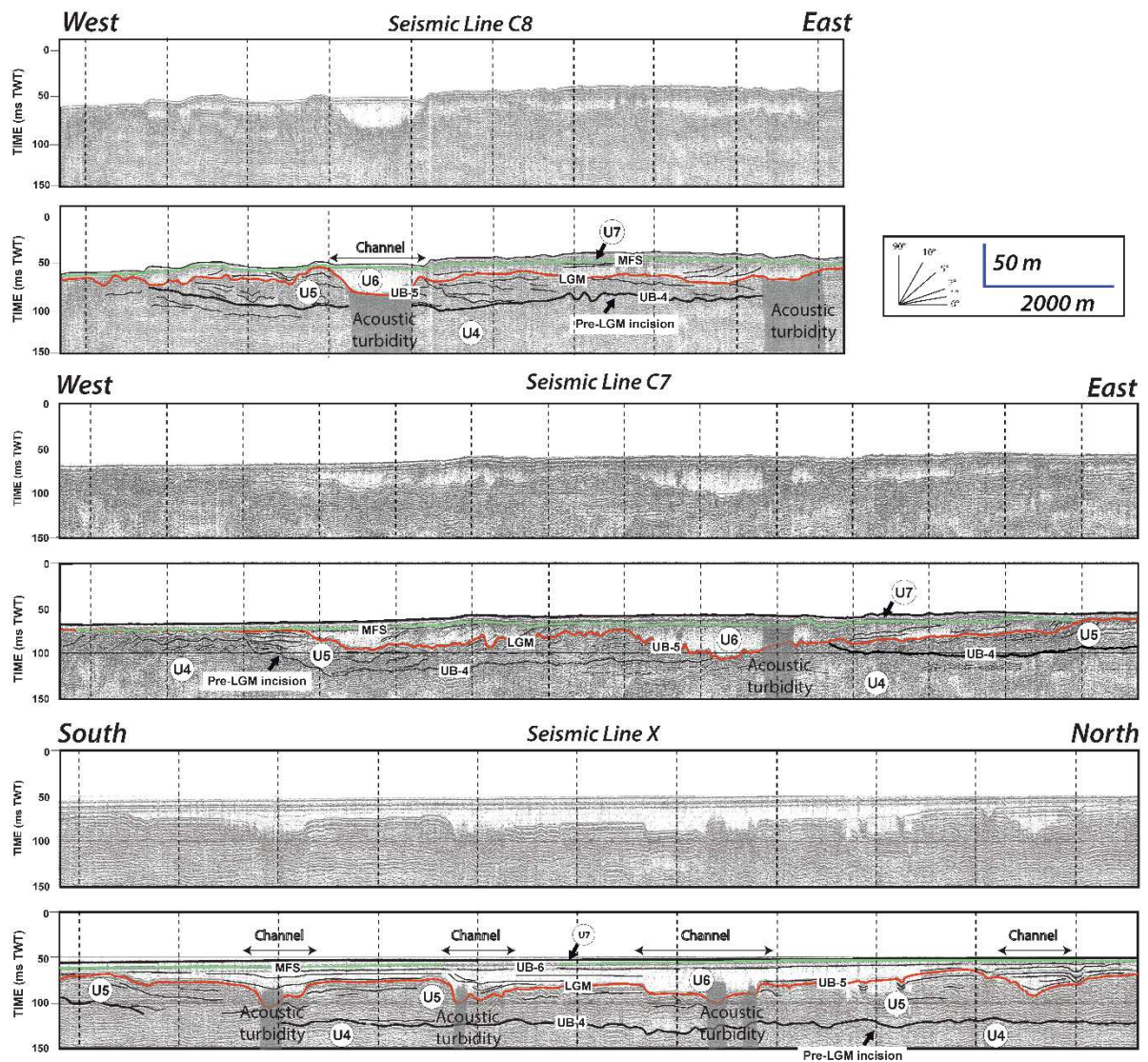
757 **Figure 3.** Map showing the bathymetry and morphobathymetric features of the Java Sea and  
 758 the Indian Ocean. Also shown is the drainage basins and the fluvial network of Java. Note the  
 759 large drainage basins in the north and the smaller basins in the south. The southeastern limit  
 760 of the Sunda Shelf is visible at the ~110 m



761

762 **Figure 4. A:** Sparker 2D High Resolution Seismic profile L-42. The profile passes through  
 763 cores BH-02 and BH-07, south to north in the Jakarta Bay. Vertical scale in two-way travel

764 time in seconds (TWTs). The scale in meters is established for sediments with P-wave velocity  
 765 of 1600 m/sec. Note that the light blue coloured packages within U3 indicate the head of several  
 766 deltaic lobes that are stacked and extends laterally. **B:** Sparker 2D High Resolution Seismic  
 767 profile CL-06, west to east in the Jakarta Bay. Vertical scale in two-way travel time in seconds  
 768 (TWTs). The scale in meters is established for sediments with P-wave velocity of 1600 m/sec.  
 769



770

771 **Figure 5.** Sparker 2D High Resolution Seismic profiles C-8, C-7 and C-X. The profile C-8 is  
 772 located in. Vertical scale is in two-way travel time in seconds (s TWT). The scale is in meters  
 773 and is established for sediments with P-wave velocity of 1600 m/sec.

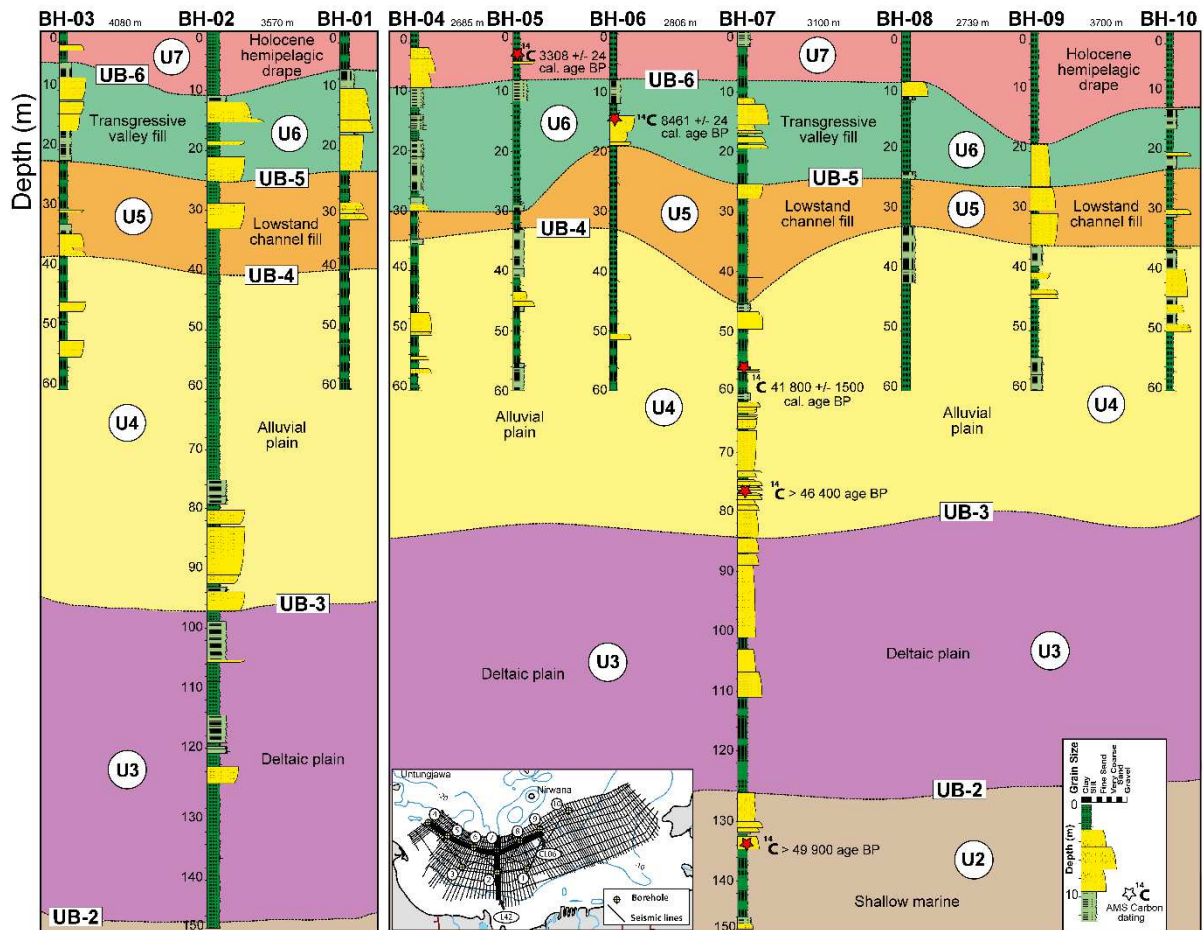
774

775

776

777

778



779

780 **Figure 6.** Stratigraphic correlation of the facies types recognized in the sediment cores and  
781 interpretation of corresponding depositional environments. Also shown are the stratigraphic  
782 positions of samples used for AMS <sup>14</sup>C dating.

783

784

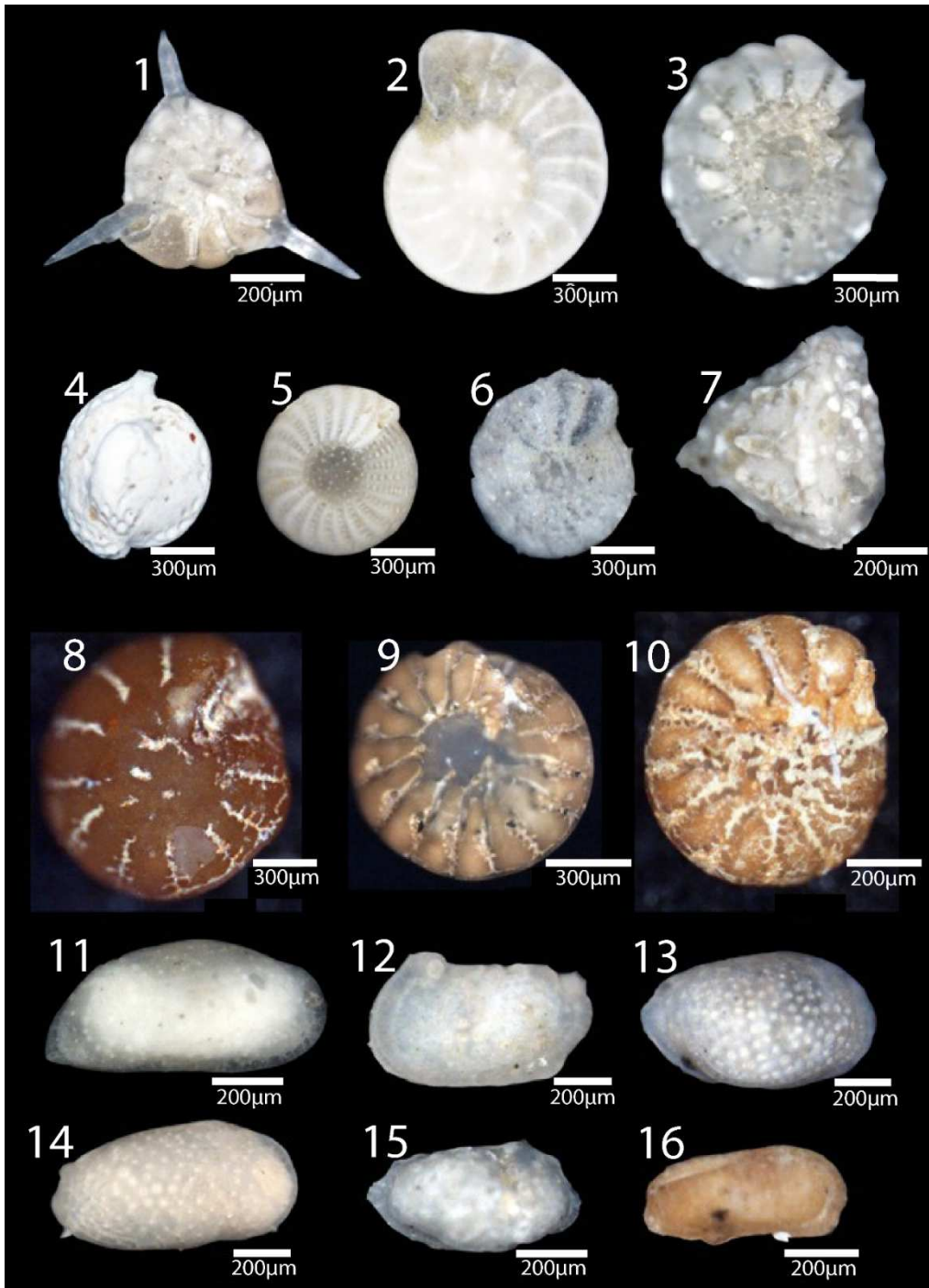
785

786

787

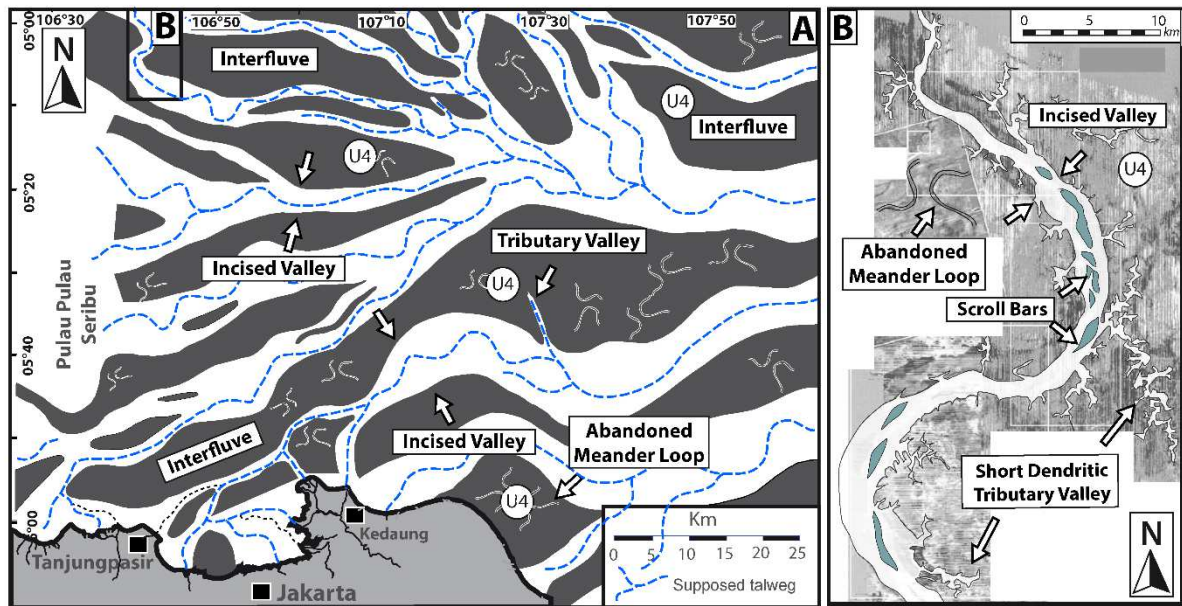
788

789



790

791 **Figure 7.** Microfossil assemblages that aided in the interpretation of the depositional  
 792 environments of the sediments. Benthic foraminifera: 1. *Asterorotalia*; 2. *Operculina*; 3 & 7  
 793 *Pseudorotalia*; 4. *Quinqueloculina*; 5 & 6. *Elphidium*; 8-10. *Ammonia yabei*. Ostracoda: 11.  
 794 *Phlyctenophora*; 12. *Neocytheretta*; 13. *Loxoconcha*; 14. *Keijella*; 15. *Neomonoceratina*; 16  
 795 *Hemicytheridea*



796

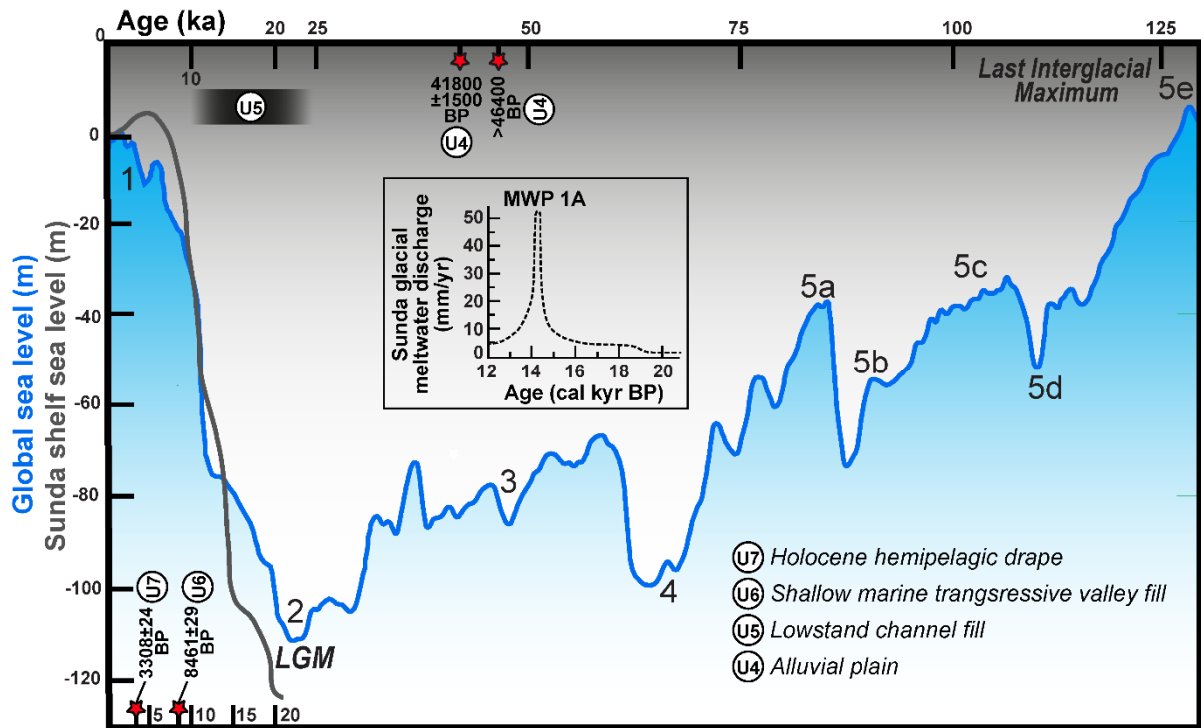
797 **Figure 8. A:** Reconstructed paleochannel network of the offshore Java Sea based on High  
 798 Resolution seismic profiles shown in Figure 1B. **B:** Time slice from the north of the study  
 799 area at ~72 m subsea showing the principal trunk incised valley and associated components of  
 800 the fluvial system such as incised dendritic tributary valleys, scroll bars and abandoned  
 801 meander loops. Figure modified and location from Posamentier (2001)

802

803

804

805

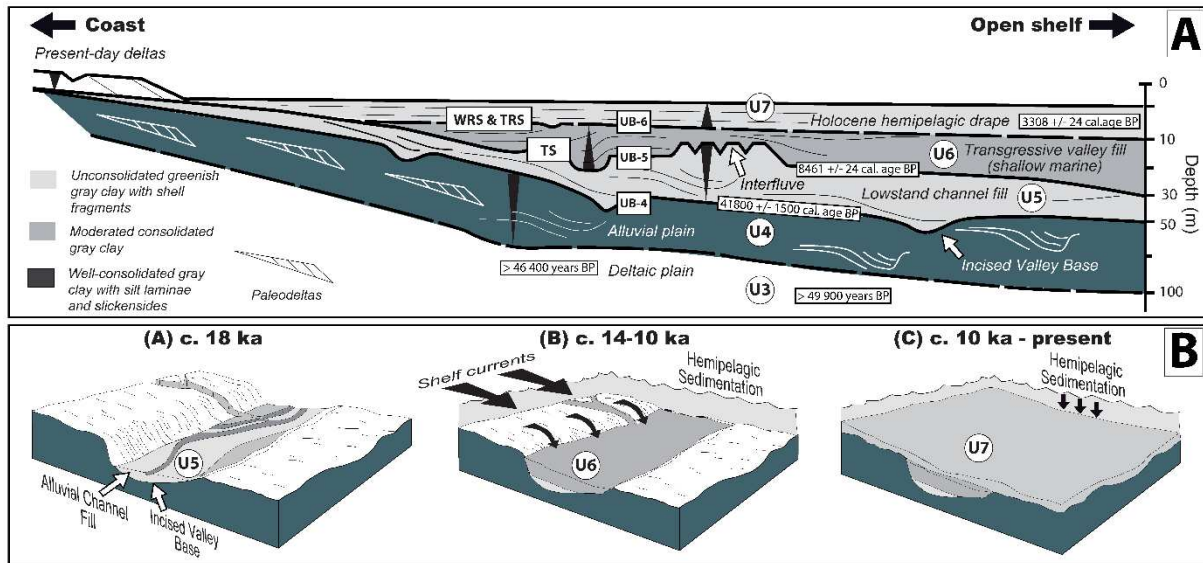


806

807 **Figure 9.** Regime diagram showing the global eustatic sea level and Sunda shelf sea level  
 808 curve for the past 125 ka and 20 ka, respectively, along with timing of the major Marine  
 809 Isotopic Stages (1–5) and the Last Glacial Maximum. Sunda shelf sea-level curve is adapted  
 810 from Twarog et al. (2021). Red stars indicate the calibrated ages of sedimentary units (shown  
 811 with white circles and U7–4) from  $^{14}\text{C}$  radiocarbon dating of shells, shell fragments and  
 812 sediments.

813





814

815 **Figure 10. A:** Present-day sedimentary architecture of the northern Java Sea. **B:** Schematic  
 816 depiction of the evolution of incised valley fill in Java Sea, modified from Posamentier  
 817 (2001). It shows from the time of maximum sea level lowstand, (A) sedimentation was  
 818 characterized by fluvial deposition, (B) followed by rapid transgression and filling by traction  
 819 and hemipelagic sedimentation, and finally, (C) the time of sea-level highstand and deposition  
 820 of hemipelagic drape over the entire area.

821

822

823

824

825

826

827

828

830 **Table 1. Locations, water depth and lengths of sediment cores recovered from the the**  
 831 **Jakarta Bay and analysed in this study**

Core	Core length (m)	Water depth (m)	Coordinates		
			WGS_1984_UTM_Zone_48S X (m)	Y (m)	Latitude (S) Longitude (N)
1	60	15.31	704259.24	9330033.60	6°3'28.92" 106°50'43.98"
2	150	14.72	700755.12	9329627.65	6°3'42.52" 106°48'50.09"
3	60	13.76	696699.08	9330108.06	6°3'27.30" 106°46'38.15"
4	60	14.46	692826.95	9335232.98	6°0'40.92" 106°44'31.67"
5	60	15.27	695034.37	9333810.38	6°1'26.97" 106°45'43.62"
6	60	16.54	697886.62	9332414.95	6°2'12.11" 106°47'16.50"
7	150	17.36	700646.47	9332020.42	6°2'24.64" 106°48'46.28"
8	60	18.23	703556.3	9334974.58	6°1'49.40" 106°50'20.78"
9	60	19.59	705541.07	9334974.41	6°0'47.30" 106°51'25.11"
10	60	20.49	708651.68	9336919.69	5°59'44.30" 106°53'6.01"

832

833 **Table 2. AMS <sup>14</sup>C dating of shells, shell fragments and sediments retrieved from the**  
 834 **cores**



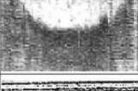
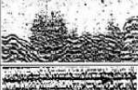
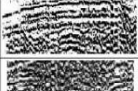
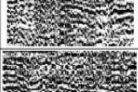

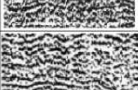
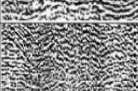








Core	Lab number	Depth (mbss)	Seismic Unit	$\delta^{13}C$ value	Age ( <sup>14</sup> C years BP)	Material
BH-05	X32132	7	U7	3.5	3308±24	Shell
BH-06	X32133	14.3	U6	-4.0	8461±29	Shell
	X31404	56.2	U4	-29.1	41800±1500	Sediment and shell fragments
BH-07	X31405	77.00	U4	-19.2	>46400	Sediment and shell fragments
	X31406	134.45	U2	0.8	>49900	Sediment and shell fragments

835

836

837

838

Unit	Facies	Illustration	Continuity	Amplitude	Frequency	Reflector Configuration	Interpretation
U-7	F-7A		Good	Good	Medium	Aggrading parallel	Marine muds
	F-7B		Medium	Good	Medium	Aggrading parallel	Channel fill
U-6	F-6A		Poor	Very poor	Low	Transparent	Channel infill polymix
	F-6B		Poor	High	Low	Acoustic turbidity	Gas-charged sediments
	F-6C		Poor	Medium	High	Aggrading parallel	Bars associated to channel migration
U-5	F-5A		Very poor	Medium	Low	Acoustic turbidity	Gas-charged sediments
	F-5B		Poor	Medium	High	Oblique-aggrading subparallel	Channel bars system
	F-5C		Poor	High	High	Oblique-aggrading subparallel	Channel bars system
U-4	F-4A		Medium	Medium	High	Aggrading subparallel	Bars associated to channeling drainage system
	F-4B		Poor	Medium	Medium	Acoustic turbidity	Gas-charged sediments
	F-4C		Poor	Poor	Medium	Irregular Oblique-aggrading subparallel	Bars associated to channeling drainage system
U-3	F-3A		Medium	Medium	Medium	Aggrading subparallel	Marine muds and sandy intercalation
	F-3B		Very poor	Medium	Medium	Acoustic turbidity	Gas-charged sediments
U-2	F-2A		Medium	Medium	Low	Aggrading folded parallel	Marine muds
	F-2B		Very poor	Medium	Low	Acoustic turbidity	Gas-charged sediments
U-1	F-1A		Low	Medium	Low	Aggrading subparallel	Marine sediments
	F-1B		Very poor	Low	Low	Acoustic turbidity	Gas-charged sediments

